

JET NOISE REDUCTION USING PULSED FLUIDIC ACTUATION

Rémy Maury, André Cavalieri, Peter Jordan, Joel Delville, Jean-Paul Bonnet

Institut Pprime-Branche fluide

Université de Poitiers

43 route de l'aérodrome, 86000 Poitiers, France

remy.maury@etu.univ-poitiers.fr, andre.cavalieri@univ-poitiers.fr,

peter.jordan@univ-poitiers.fr, jean-paul.bonnet@univ-poitiers.fr, joel.delville@univ-poitiers.fr

ABSTRACT

Steady and unsteady fluidic actuators, in the form of secondary control jets injecting from the nozzle lip, aimed at jet noise reduction, are investigated. Three different geometric configurations are tested: non-converging control jets, 'open' triangle convergence and 'closed' triangle convergence. By means of a triple decomposition of hot-wire data and a scale-separation argument, the low-frequency perturbation (near-nozzle dynamics) and response (global, downstream dynamics) of the flow are studied. Comparison of the phase-averaged component of the decomposition with predictions of linear stability theory (LST) suggest that two qualitatively different responses are active: at the main forcing frequency the jet response looks to be non-linear; at two secondary, higher frequencies, LST gives reasonable predictions for the local growth rates and convection velocities.

INTRODUCTION

This paper investigates the response of a single-stream round turbulent jet to steady and unsteady fluidic actuation. The actuation comprises an azimuthal distribution of 16 nozzle-lip mounted microjets, injecting at a penetration angle (defined in the $x-r$ plane, with respect to the jet axis) of 60° . Three geometrical configurations are explored by varying the convergence angle, measured with respect to the $x-r$ plane, and the distance between the microjets: (1) equispaced, non-converging microjets; (2) microjets that converge (angle measured with respect to the $x-r$ plane) in pairs so as to form a 'closed' fluidic triangle that 'pinches' the main jet; (3) an intermediate configuration comprising microjets that converge in pairs so as to form an 'open' fluidic triangle. The response of the flow is assessed in terms of both the flow structure and the acoustic radiation, systematic comparisons being performed between the three geometrical variants, for both steady and unsteady actuation, the latter being effected at a Strouhal number of $St_D = 0.15$

The actuated flows are assessed in terms of the near-nozzle (local) and downstream (global) responses. By appealing to a scale separation, the former (dominated by localised, non-linear mechanisms—high-frequency, small-scale) is in-

terpreted as a 'perturbation' where the global downstream response is concerned. Data acquired by means of hot-wire measurements are analysed in the context of a triple-decomposition, and the phase-averaged component is compared with spatial linear stability theory of Michalke (1971). Results indicate that while the global response of the jet to the main forcing frequency ($St_D = 0.15$) is non-linear, the response at two other frequencies present in the 'perturbation' ($St_D = 0.3, 0.45$) shows reasonable agreement with LST in terms of both the local growth rate and the convection velocity.

1 Experiment and measurement procedures

The experiments were performed in the anechoic jet-noise facility 'Bruit et Vent' ('Noise and Wind') at the CEAT (Centre d'Etudes Aérodynamiques et Thermiques) in Poitiers. The Mach and Reynolds numbers of the jet studied are, respectively, $M = 0.42$ and $Re = 7.4 \times 10^5$. The boundary layer is tripped upstream and fully turbulent at the exit. The main and control jet diameters are, respectively, $D = 80$ mm and $d = 2.1$ mm. The penetration angle, which is the angle, measured in the $x-r$ plane, between the microjet axis and the main jet axis, is $\alpha = 60^\circ$. The convergence (or yaw) angle, measured with respect to the $x-r$ plane, is $\theta = 40^\circ$. Figure 1(a) and (b) show a schematic of the control jets and a photograph of the 'closed' triangle configuration.

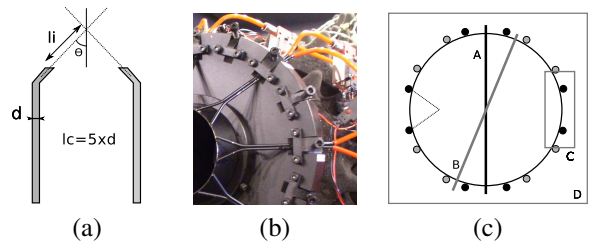


Figure 1. (a) Schematic of a pair of control jets, with convergence angle; (b) photo of 'closed' triangle configuration, $l_i < l_c$; (c) measurement planes

The ‘open’ and ‘closed’ triangle configurations are so named for the following reason. If we consider as a nominal effective penetration length the length of the potential core of the control jets, $l_c = 5d$, a ‘closed’ fluidic triangle is formed when the geometric intersection length (l_i in figure 1) is lower than l_c : $l_i < l_c$. If, on the other hand, $l_i > l_c$, we can consider that the fluidic injection does not form such a ‘closed’ triangle, the control jets behaving, in this situation, in more independent manner, similar to the non-converging microjets.

For the unsteady actuation, microjets are pulsed, in phase, by means of *Dynamco*TM valves. Each valve is driven by a square wave with pulsation frequency of 280 Hz ($St_D = 0.15$). The mass flow rate of the sixteen microjets is controlled and measured using an integrated mass flow controller and meter; the mass flow varies between 0% and 1.8% of the main jet flow rate.

Acoustic measurements were performed with 8 microphones positioned on an arc at $x/D=31$ and between 30 and 100 degrees (with respect to the downstream jet axis). The flow is measured using a single hot-wire ($2.5 \mu\text{m}$), sampled at 250 kHz. An *in-situ* calibration of the hot-wire is performed (technique described in Tutkun *et al.* (2008)). The jet is probed in two $x-r$ planes (A and B in figure 1(c)), one in the control-jet ‘intersection’ plane, the other between two pairs of control jets; in the non-converging case, the measurement planes are the injection plane and the plane between two control jets. The section C corresponds to the near-nozzle microjet interaction.

2 Acoustic results

Acoustic results are here presented for the ‘open’ triangle configuration only. The noise reduction produced by steady and pulsed actuation is shown in figure 2, as a function of frequency and emission angle. Reductions of up to 3dB are achieved by steady actuation, the largest reduction being observed at high emission angle and over a frequency range $0.4 < St_D < 1$. When the actuation is pulsed, the noise reduction is more modest, and localised regions of noise increase are observed in the pulsed configuration, in the vicinity of the pulsation frequency, $St_D = 0.15$, and at $St_D = 0.3$.

3 Aerodynamic results

The aerodynamic results are organised as follows. We first assess the impact of the steady and unsteady fluidic actuation on the mean-flow structure and the fluctuation levels. We then perform a triple decomposition of the velocity measurements, $u = U + \tilde{u} + u'$, where U is the time-averaged component of the flow, \tilde{u} the phase-averaged component (which is further decomposed into the three most energetic frequencies observed in the measurements: $St_D = 0.15, 0.3$ and 0.45), and u' , the background turbulence.

Following the triple decomposition, we propose the following conceptual framework for analysis and interpretation of the results. The fluid dynamics in the interaction region, where the control jets impinge on the main jet, are characterised by high-frequency, fine-scale unsteadiness, where non-linear mechanisms are certain to dominate; the complexity of the dynamics in this region, at these scales, is such that a single hot-wire will not provide much insight, beyond giving an

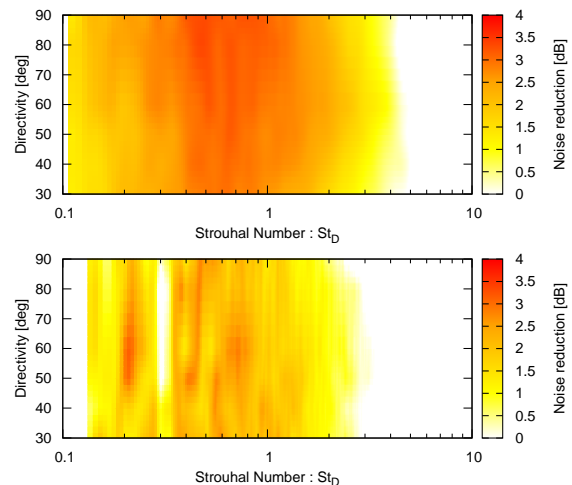


Figure 2. Far field reduction produced by control. (a) steady injection; (b) pulsed injection. White corresponds to a noise increase.

indication of the structure of the mean field and the fluctuations. However, as the perturbation frequency we impose is low with respect to the said scales, a scale separation exists. Based on this scale separation we consider the fine-scale near-nozzle phenomena as being predominantly decisive in determining the spatial characteristics of the low-frequency perturbation. By means of phase-averaging the hot-wire measurements in the near-nozzle region (performed in the $r-\theta$ plane), the space-time structure of the low-frequency perturbation is extracted from the measurement; this is then interpreted as a ‘perturbation’ field, $\tilde{u}_p(r, \theta, t_\phi)$ (which can be further assessed by means of Fourier transforms in both the azimuthal and temporal directions $\tilde{u}_p(r, m, \omega_\phi)$), with respect to the large-scale response of the jet in the downstream region (also educed by means of phase-averaging); i.e. we ask the question: What is the nature (kinematic and dynamic) of the coherent structures generated in response to this low-frequency perturbation?

3.1 Mean and fluctuation fields

In this section we examine the first and second order statistical moments of the velocity field for baseline and controlled cases, for both steady and unsteady actuation.

3.1.1 Steady injection First let us consider **The near-nozzle, interaction zone**: measurements performed in the $r-\theta$ plane at $x/D = 0.1$. The structure of the mean and *rms* velocity fields in the near-nozzle region, for the baseline and three actuation geometries, is shown in figures 3 and 4. The ‘closed’ triangle configuration can be seen to ‘pinch’ the main jet, causing an ejection and turbulence of fluid exiting from the main-jet nozzle, resulting in the production of localised, turbulent co-flows, consistent with the analysis of Laurendeau *et al.* (2008). The ‘open’ triangle and non-converging configurations produce more azimuthally-homogeneous deformations of the mean field; it is also worth noting that the non-converging configuration produces the highest fluctuation levels, possibly asso-

ciated with the efficient generation of longitudinal vorticity, as reported, for example, by Alkislar *et al.* (2007) and Castelain *et al.* (2007).

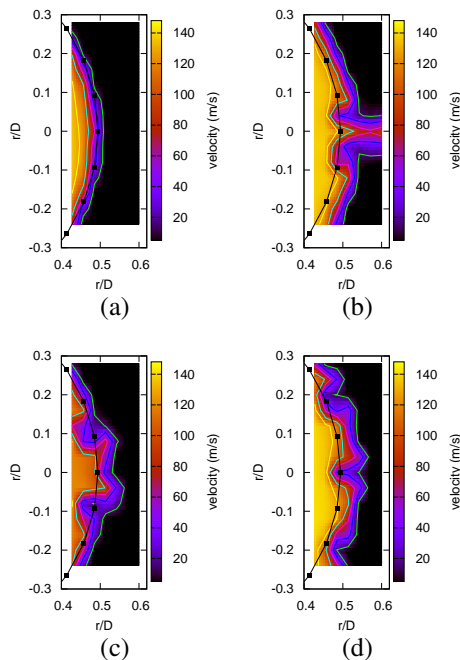


Figure 3. Structure of mean velocity field, in a section of the $r - \theta$ plane, for: (a) baseline; (b) ‘closed’ triangle actuation; (c) ‘open’ triangle actuation; (d) non-converging configuration.

The global effect of the actuation is shown in figures 5 and 6. All three configurations can be seen to produce a global reduction in the fluctuation levels and a corresponding increase in the length of the potential core. A difference is observed between the ‘closed’ triangle configuration on one hand, and the ‘open’ triangle and non-converging configurations on the other: the ‘closed’ triangle produces a lesser lengthening of the potential core. Further to this, it produces slightly higher fluctuation levels on the low-speed side of the shear-layer, and slightly reduced fluctuation levels on the shear-layer axis. The former effect can be associated with the aforesaid ejection and turbulence of main-jet fluid caused by the ‘pinching’ action of the ‘closed’ triangle configuration; this effect has been further discussed by Laurendeau *et al.* (2008). The spread-rate of the jet, as measured by the axial variation of the vorticity thickness, $\delta_\omega(x)$ shows how, downstream of $x/D = 2$, the spread-rate of the controlled jets is less than that of the baseline flow.

3.1.2 Pulsed injection The change produced in the mean and *rms* structure of the jet when the fluidic injection is now pulsed, and which is summarised in figures 7 and 8, is quite different from that produced by steady injection. The ‘closed’ configuration again shortens the potential core, while the two others lengthen it; however, all controlled jets have axial velocity profiles that remain closer to the baseline than when steady actuation is implemented; this trend is also

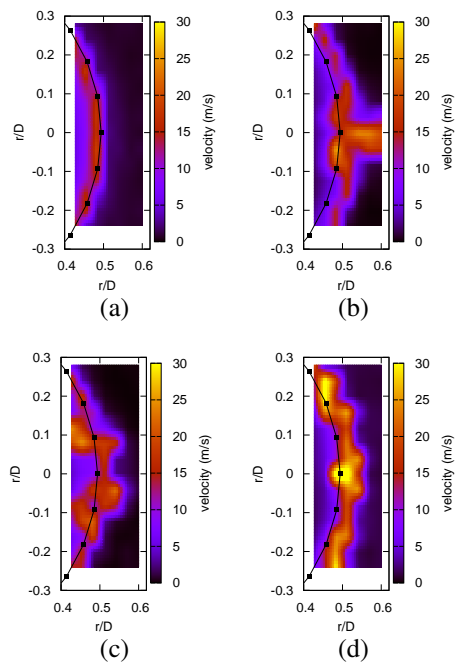


Figure 4. Structure of *rms* velocity field, in a section of the $r - \theta$ plane, for: (a) baseline; (b) ‘closed’ triangle actuation; (c) ‘open’ triangle actuation; (d) non-converging configuration.

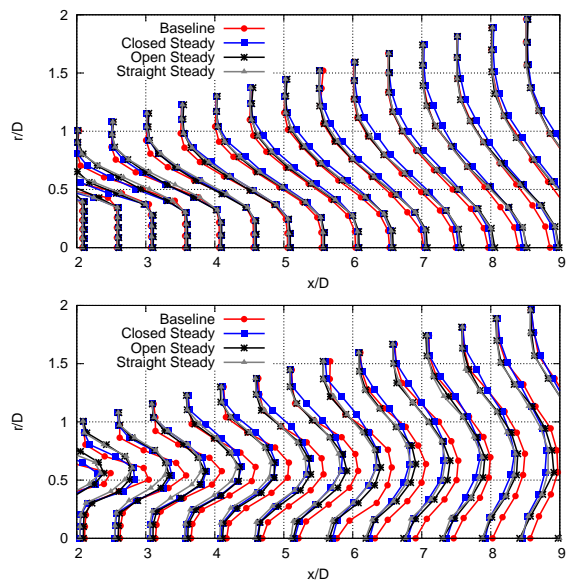


Figure 5. Top: Mean centerline streamwise velocity as a function of x/D for un-controlled and all steady controlled configurations; bottom: impact of steady actuation on structure of *rms* velocity field.

reflected in the spread-rates (compare figures 6 and 7).

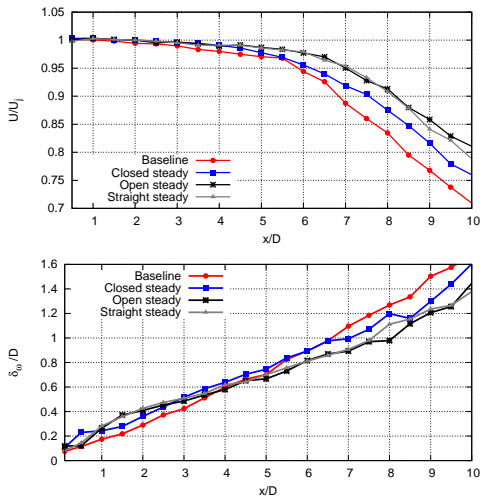


Figure 6. Top: Impact of steady actuation on the potential core length. Bottom: Comparison of δ_w/D for un-controlled and all steady controlled configurations

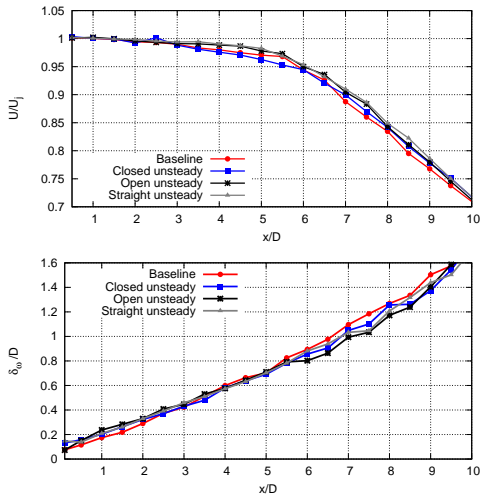


Figure 7. Top: Mean centerline streamwise velocity as a function of x/D for un-controlled and all unsteady controlled configurations; bottom: Comparison of δ_w/D for un-controlled and all unsteady controlled configurations.

3.2 Analysis via triple decomposition

As outlined above, we consider the phase-averaged component of the velocity field in the near-nozzle region as a perturbation that elicits a global large-scale response from the jet. Some preliminary comparisons are then made between the latter and linear stability theory (LST).

3.2.1 The ‘perturbation’ The control signal is a square wave, and the response of the valve and injection system is such that the frequency spectrum (measured but not shown) of the fluidic excitation contains energy at $St_D = 0.15$, $St_D = 0.3$ and $St_D = 0.45$.

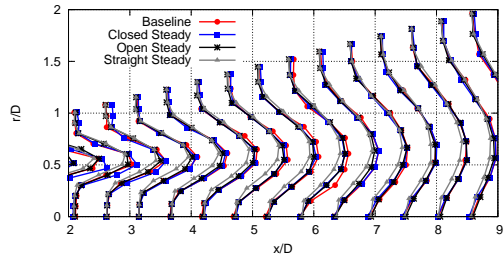


Figure 8. Impact of unsteady actuation on *rms* of velocity field.

Figure 9 shows the *pseudo*-time evolution (3 phase angles shown) of the three pulsed actuations over a half-cycle, from $\phi = 0$ to $\phi = \pi$; the second half of the cycle, from $\phi = \pi$ to $\phi = 2\pi$ is more-or-less the reverse of the first half, i.e. the perturbation is symmetric about $\phi = \pi$. It is worth noting the similarity between the maximally-deformed field (at $\phi = \pi$) and the structure of the near-nozzle mean field observed when steady actuation is implemented; this similarity supports the scale-separation evoked earlier.

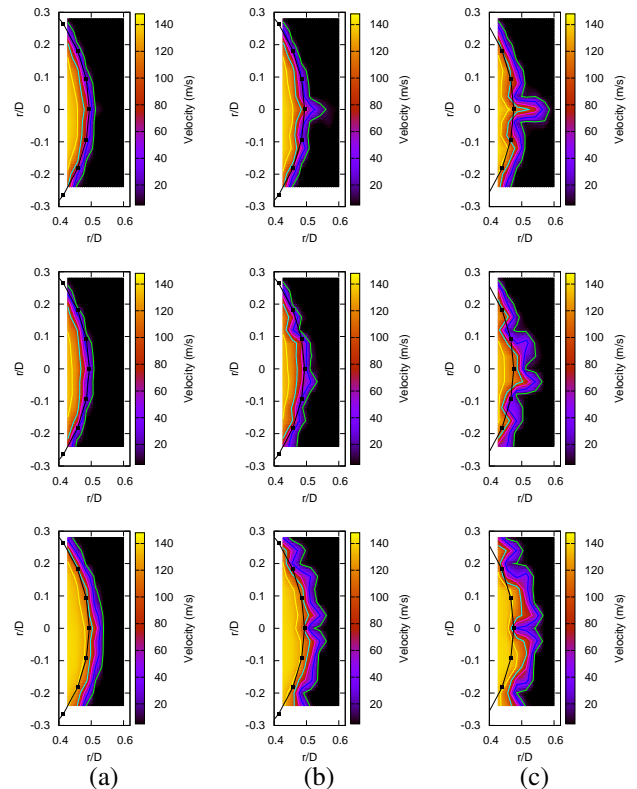


Figure 9. *Pseudo* time-evolution of the phase-averaged near-nozzle field, the ‘perturbation’. Top: ‘closed’ triangle; middle: ‘open’ triangle; bottom: non-converging configuration. (a) through (c) shows evolution between $\phi = 0$ and $\phi = \pi$ in steps of $\pi/2$.

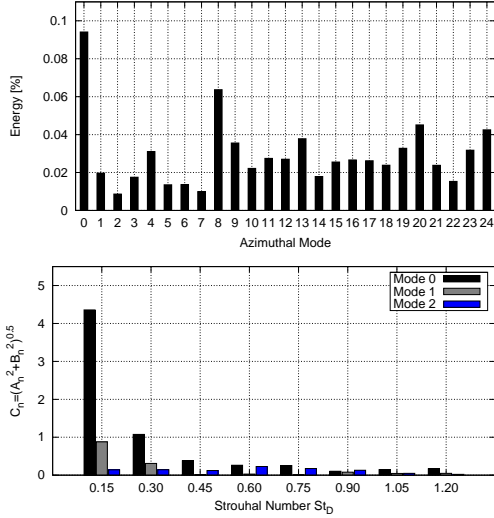


Figure 10. Top: Azimuthal spectrum $\tilde{u}_p(m)$; Bottom: $\tilde{u}_p(m=0, m=8, St_D)$.

The perturbation field so obtained is decomposed in Fourier series in both time and azimuthal angle. The azimuthal spectrum is shown in figure 10 for the ‘open’ triangle configuration. The four most energetic modes are modes $m=0$, $m=4$, $m=8$ and $m=16$. The frequency spectra of azimuthal modes $m=0$ and $m=8$ are also shown: most of the energy is concentrated at $St_D=0.15$, the components at $St_D=0.3$ and $St_D=0.45$ having approximately 75% less fluctuation energy.

3.3 The large-scale response

The ‘large-scale’ response of the flow to the perturbation is obtained by means of phase averaging. As the spectra (not shown) indicate that the response comprises three main frequencies, the phase-average is further decomposed into three components: one at $St_D=0.15$, one at $St_D=0.3$ and a third at $St_D=0.45$. Figures 11 show, for each of these, for the ‘open’ triangle configuration, the spatial structure of the response at the 4 phase angles $0, \pi/2, \pi, 3\pi/2$.

Finally, with a view to better understanding the dynamic nature of the response of the jet at these three frequencies we consider the spatial amplification of the perturbation at each frequency, the corresponding convection velocities, and we compare these with predictions made using spatial linear stability theory (Michalke (1971)) for an axisymmetric mixing-layer. The stability calculations are based on the local mean velocity profile. Figure 12 and table 1 show the results. The growth rate predicted by LST is shown at $x/D=0.5$, $x/D=1$, $x/D=2.5$ and $x/D=4.5$. For the $St_D=0.45$ case we see that the LST curve ($e^{\alpha x}$) is tangent to the experimental curves for the first three positions, after which LST shows this frequency to be stable; this is where the experimental amplitudes begin to decay. At $St_D=0.3$, in the initial region agreement with LST is poor, downstream of $x/D=1$, however, the LST curves are again tangent to the experimental curves. For the lowest frequency component, while the LST curves appear to align with the experimental curves at $x/D=2.5$ and

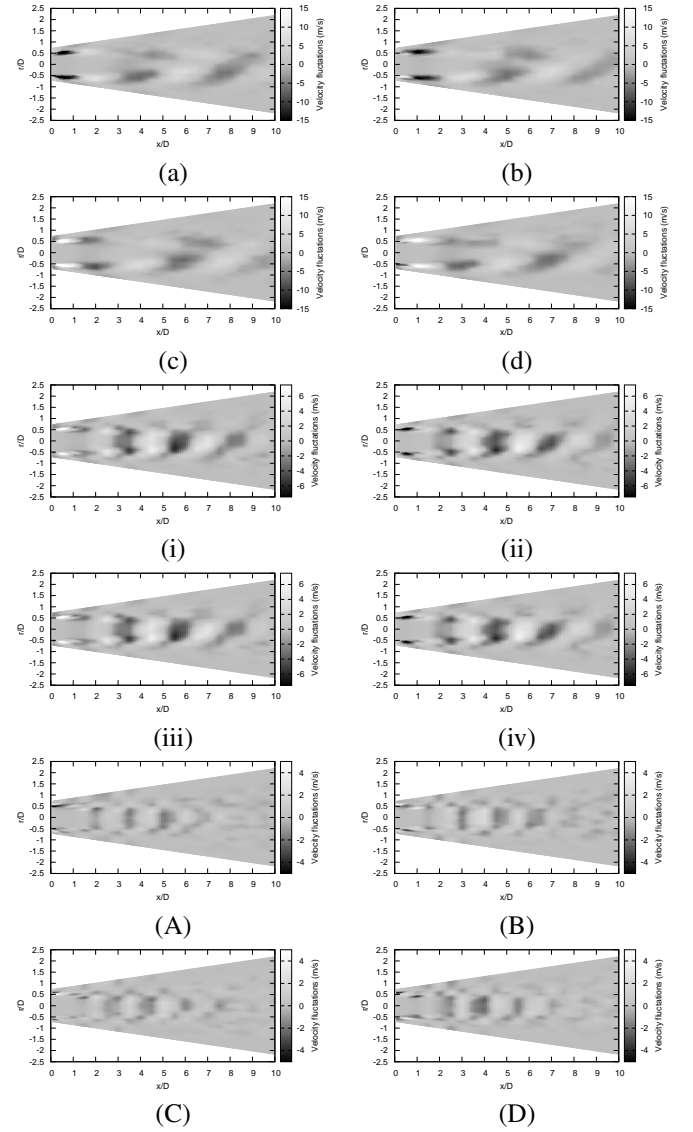


Figure 11. Phase averaged response of the jet at $St_D=0.15$ (a-d), $St_D=0.3$ (i-iv) and $St_D=0.45$ (A-D) to ‘open-triangle’ fluidic forcing; four phase angles shown in each case $\phi=0$, $\phi=\pi/2$, $\phi=\pi$ and $\phi=3\pi/2$.

$x/D=4.5$, the large discrepancy in the convection velocity suggests that this component of the jet response is not synonymous with LST, and is non-linear. This is consistent with the very large forcing amplitudes at this frequency.

Strouhal Number : St_D	0.15	0.30	0.45
Theoretical U_c	0.95	0.86	0.70
Experimental U_c	0.40	0.77	0.83

Table 1. Comparison between the averaged convection velocity U_c of LST and ‘Open’ triangle configuration.

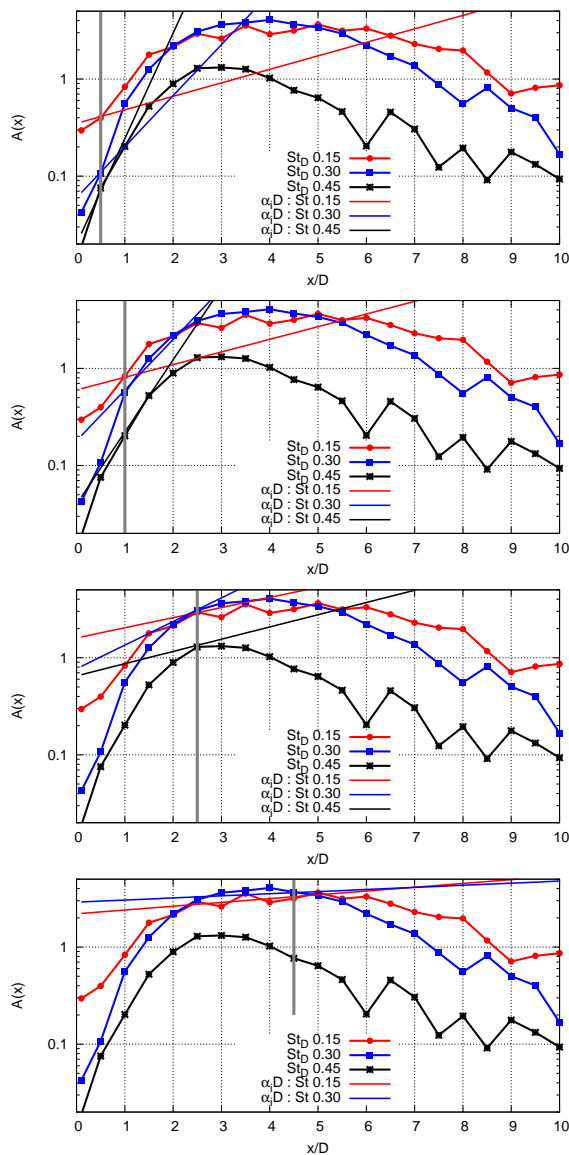


Figure 12. Comparison of spatial evolution of the radially-integrated, phase-averaged velocity amplitude, $A(x)$, with predictions of linear stability theory (LST) based on the local mean velocity profiles at $x/D = 0.5$, $x/D = 1$, $x/D = 2.5$ and $x/D = 4.5$. The vertical line in each subfigure indicates the position at which the LST is performed; and the red, blue and black exponentials, $e^{\alpha x}$, show the LST prediction.

4 Conclusions

The response of a subsonic jet to steady and unsteady fluidic forcing is explored. The main results are: (1) steady and unsteady forcing produce quite different changes in the first and second order statistical moments of the velocity field: the lengthening of the potential core and associated reduction in spreading rate observed for steady injection are no longer so marked; (2) the response of the flow to unsteady forcing appears to comprise a non-linear component, at the main forcing frequency, and two secondary components which may be explicable in the context of linear stability theory.

5 Acknowledgements

This work was partially funded through the EU seventh Framework Program (FP7/2007-2013) under the program OPENAIR (grant agreement 234313) and the EU-Russian program ORINOCO (FP7-AAT-2010-RTD-Russia; project number 266103) and Airbus. The authors also gratefully acknowledge the helpful input of Jerome Huber from Airbus Operations SAS (“Acoustics and Environment Department”) and Damien Biau from the Pprime Institute.

REFERENCES

- Alkislal, M.B., Krothapalli, A. & Butler, G.W. 2007 “the effect of streamwise vortices on the aeroacoustics of a mach 0.9 jet”. *Journal of Fluid Mechanics* **Vol. 578** (01), 139–169.
- Castelain, T., Sunyach, M., Juv, D. & bra, J.C. 2007 “jet noise reduction by impinging microjets: an aerodynamic investigation testing microjets parameters”. In *13th AIAA/CEAS Aeroacoustics Conference (28th AIAA Aeroacoustics Conference)*, , vol. 2007-3419. Rome, Italy.
- Laurendeau, E., Jordan, P., Bonnet, J.P., Delville, J., Parnoudeau, P. & Lamballais, E. 2008 “subsonic jet noise reduction by fluidic control: The interaction region and the global effect”. *Physics of fluids* **Vol.20, No.1**, pp.1-15.
- Michalke, A. 1971 Instability of a compressible circular free jet with consideration of the influence of the jet boundary layer thickness. *Z. fur Flugwissenschaften, (West-Germany)* **19** (8), 319–328.
- Tutkun, M., George, W.K., Foucaut, J.M., Coudert, S., Stanislas, M. & Delville, J. 2008 “in situ calibration of hot wire probes in turbulent flows”. *Experiment in Fluids* **Vol. 46**, (617–629).